Journal of Magnetism and Magnetic Materials 497 (2020) 166068

Contents lists available at ScienceDirect

Journal of Magnetism and Magnetic Materials

journal homepage: www.elsevier.com/locate/jmmm

Non-conventional ferromagnetism and high bias magnetoresistance in TiO_{2-x}: A simple phenomenological approach

V.Z.C. Paes[a], D.H. Mosca[a], A.J.A. de Oliveira[b], J. Varalda[a,*]

[a] Departamento de Física, Universidade Federal do Paraná, 81531980 Curitiba, Paraná, Brazil
[b] Departamento de Física, Universidade Federal de São Carlos, Rod. Washington Luis, Km 235, 13565-905 São Carlos, São Paulo, Brazil

ARTICLE INFO

Keywords:
Nonconventional ferromagnetism
Tunnel magnetoresistance
Oxygen-defective TiO_2

ABSTRACT

A simple phenomenological approach is used to describe magnetization and magnetoresistance in thin films of oxygen-deficient rutile titanium dioxide (TiO_2). Magnetization curves were successfully simulated by considering the ferromagnetic (FM) contribution of magnetically interacting oxygen vacancies (VO's) forming a single-domain using the Stoner-Wohlfarth (SW) model combined with paramagnetic (PM) contribution of isolated VO's described by a Langevin function. Whereas approximately half of the VO's behave as ferromagnetically coupled, rotating coherently with the applied magnetic field, the remaining half of the VO's tend to align individually with the local magnetic field overcoming the thermal fluctuation deviations. The conduction mechanism is described by variable range hopping (VRH) regime with electron hopping between VO's centers in the TiO_{2-x} matrix. The magnetoresistance (MR) curves are consistently simulated through the scaling with square of PM contribution of magnetization, indicating that resistance depends on the relative orientation of the magnetic moments associated with non-interacting VO's dispersed in TiO_2 matrix at low temperatures. Density functional theory (DFT) calculations were performed to validate the parametrization of the phenomenological approach used to described the ferromagnetic groundstate of the V_O network and spin polarization in the VRH regime in the TiO_{2-x} matrix. Spin-resolved density of states (DOS) calculations consistently reveal that magnetoresistance can be ascribed to electron hopping from defect-states located immediately below Fermi level to the bottom of conduction band states with an opposed spin-polarization.

1. Introduction

Metal oxides are versatile materials and continuing breakthroughs in their synthesis and modifications in nanoscale have brought new properties and new applications. Particularly, TiO_2 is among the most widely used metal nano-oxides in mature technologies, and so, their non-conventional ferromagnetism appears as a new and promising property [1–3].

The magnetic moment formation and their interconnectivity of non-conventional ferromagnetism observed in oxygen-defective undoped TiO_2 films is still debated, but there exists a consensus that it is straightly related with native point defects, which are mainly titanium vacancies and oxygen vacancies (VO's). Experimental findings have shown that the saturation magnetic moments of TiO_2 thin films decrease as the annealing time increases in an oxygen-rich atmosphere, whereas vacuum annealing enhances the magnetization. Thereby, it is suggesting that the spontaneous magnetization in undoped TiO_2 is closely related to the O vacancy instead of the Ti vacancy [1–3].

First-principles electronic structure calculations based on DFT indicate that Ti vacancy and divacancy may be responsible for magnetic moments of $3.5\mu_B$ and $2.0\mu_B$, respectively, in undoped anatase TiO_2, where ferromagnetic state is more stable than the antiferromagnetic state [4]. However, DFT calculations also indicate that VO defects can induce ferromagnetism in both rutile and anatase TiO_2 [5]. In this case, the rutile and anatase TiO_2 show magnetic moments of $0.22\mu_B$ and $0.06\mu_B$ per VO, respectively.

Additional studies suggested that, despite the titanium vacancies can cause a high-spin defect state and ferromagnetic coupling, and that VO reduces two Ti^{4+} ions into Ti^{3+} to yield a stable antiferromagnetic state [6], an alternative mechanism involving multi-defects can also produce local magnetic moments, where the electrons induced by the VO mediate long-range ferromagnetic coupling [7]. Several experimental findings confirm the ferromagnetism induced by VO in rutile TiO_2 [8], and in anatase-rutile mixed phases of undoped TiO_2 [9–11]. Furthermore, TiO_2 single crystals irradiated by oxygen ions corroborate that Ti^{3+} ions on the substitutional sites accompanied by VO provide the

* Corresponding author.
E-mail addresses: mosca@fisica.ufpr.br (D.H. Mosca), varalda@fisica.ufpr.br (J. Varalda).

https://doi.org/10.1016/j.jmmm.2019.166068
Received 1 September 2019; Received in revised form 4 October 2019; Accepted 27 October 2019
Available online 28 October 2019
0304-8853/

local moments [12].

These findings indicate that the spontaneous magnetization observed in undoped TiO_2 material is reasonably described by the VO concentration. From the electronic transport viewpoint, TiO_2 is highly resistive due to high energy gap, even in the presence of VO's which nearly full charge compensation generates a n-type semiconducting behavior. Despite the existence of different titanium oxide polymorphs, the removal of one neutral lattice oxygen atom leaves two extra electrons (assuming a formal -2 oxidation state of O in TiO_2), which will fill empty states of Ti ions. The localization of excess electrons and formation of Ti^{3+} species in rutile and anatase phase have been addressed in several theoretical works [13], revealing that it is reasonable to assume that electron-transport properties in both phases present qualitatively similar features even if specific activation barriers for hopping from one to the next Ti site might differ due to structural differences. Essentially, electrical conductivity processes are mainly due to hopping via impurity centers [14].

Next, we have demonstrated that a simple and standard minimization energy procedure can be successfully used to describe the field- and temperature-dependent magnetization. In addition, the same magnetization treatment based on the configuration of VO's is used to simulate a large negative magnetoresistance observed at high bias voltage in low temperature.

2. Experimental

TiO_2 thin films were prepared by pulsed laser deposition from nominal TiO_2 targets with a base pressure of 10^{-7} mbar on the native thin oxide layer on commercial Si(100) wafers kept at room temperature. A pulsed excimer KrF laser ($\lambda = 248$ nm, $\tau = 20$ ns) was used at a fluence of about 3 J cm^{-2} and a repetition rate of 2 Hz. The distance between the substrate and the target was 5 cm. Transmission electron microscopy (JEM 2100F microscope operating at 200 kV) was used to determine the predominant rutile crystalline structure in the films with some portions of amorphous regions which can be qualified as rutile-like. The composition of the TiO_{2-x} matrix were investigated by electron energy loss spectroscopy, indicating the composition of $TiO_{1.95\pm0.05}$ for the matrix. More details on the TiO_{2-x} films can be found in the references [15–17].

Magnetic measurements were carried out using a superconducting quantum interference device (SQUID) magnetometer (Quantum Design MPMS-5S) with the applied magnetic field parallel to the film surface.

Resistance and magnetoresistance measurements were performed with magnetic field applied in the film plane along the current lines using a Physical Property Measurement System (PPMS 6000) system. The two terminal electrical contacts made by silver paint that were spaced by about 3 mm each other.

3. Results and discussion

3.1. Magnetization of TiO_2 matrix

The non-conventional ferromagnetism of the undoped TiO_{2-x} films exhibits moderately open magnetic hysteresis loops for which saturation magnetization is almost temperature independent in the temperature range between 5 K and 300 K. In this study, the non-conventional ferromagnetism is modelled within an extended SW model for the case of a ferromagnet with a tetragonal anisotropy. The extended SW model for tetragonal FM is represented by a single magnetic domain with magnetization, $\vec{M}_{FM}$, which coherently rotates in an externally applied static magnetic field, $\vec{H}$ (see Fig. 1). This magnetization a priori corresponds to a cluster of VO's, which are magnetically coupled with each other. The total energy density is the sum of a tetragonal anisotropy energy density [18], $E_A = K_1\cos^2(\theta) + K_2\cos^4(\theta)$, and the Zeeman energy density, $E_Z = -\vec{M}_{FM}\cdot\vec{H}$, where K_1 and K_2 are the lowest order

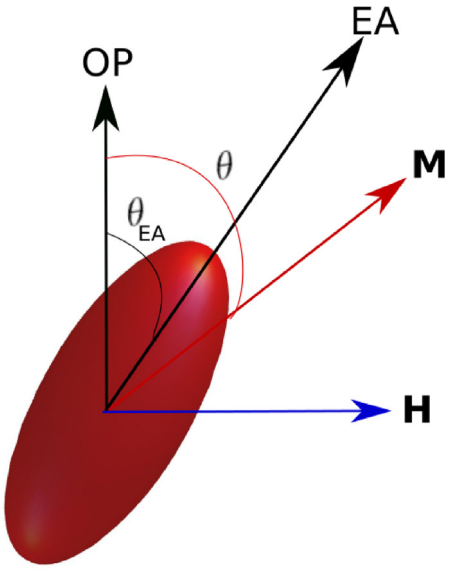

Fig. 1. Illustration of the variables used in the Stoner-Wohlfarth model. The angles θ_{EA} and θ are defined for the easy axis (EA) of the single domain with magnetization $\vec{M}$ with respect to the magnetic field $\vec{H}$ applied in the film plane, whereas *OP* is the normal out-of-plane direction.

terms of the energy density along with hard magnetic axis (directions of greatest energy) and intermediate magnetic axes (intermediate energy). Thus energy per unit volume can be expressed as:

$$E = E_A + E_Z = K_1\cos^2(\theta - \theta_{EA}) + K_2\cos^4(\theta - \theta_{EA}) - \vec{M}_{FM}\cdot\vec{H} \quad (1)$$

where E_A is minimum (zero) when $\theta = \theta_{EA}$ for $K_1 < 0$ and $K_2 > 0$. Once the easy axis (EA) is determined, the angle that the magnetic field makes with the EA is denoted as θ_{EA}.

The standard minimization procedure [19–21] to obtain the magnetization were performed using Maple 2017. At equilibrium, the ferromagnetic component of magnetization points along a direction defined by an angle θ_{min} that minimizes the total energy per unit volume.

In addition to the FM component of magnetization (M_{FM}), we consider a PM component (M_{PM}) of magnetization which takes into account the presence of free magnetic moment associated with isolated VO centers within the TiO_2 matrix. Such a PM contribution is taken as proportional to a simple Langevin function, $L_{PM}(x)$. Therefore, the total magnetization of TiO_2 matrix can be expressed as:

$$M = M_{FM} + M_{PM} = M_{FM} + M_O L(x) \quad (2)$$

where $M_O = N_O \mu_O$ is the total magnetization of the non-interacting VO centers dispersed in the matrix, N_O is the number density, μ_O is the magnetic moment of dispersed and isolated VO's, and $L(x) = \coth(x) - 1/x$ with $x = \mu_O(H + H_{eff})/(k_B T)$ the ratio of the total Zeeman energy of the isolated moments in the effective magnetic field to the thermal energy given by $k_B T$, where k_B is the Boltzmann constant), and $H_{eff} \approx N_{eff} M_{FM}$ corresponds to an effective local field exerted on the VO's due to the magnetized state of the matrix. Here, N_{eff} is the effective demagnetizing factor of the matrix. Each magnetization term, either FM or PM, contributes to the total magnetization and can be properly weighted in the simulations of the magnetic hysteresis. Even if the values of moments could differ in the diluted and percolated limits of VO concentration, a single magnetic moment value can be assumed for M_{FM} and M_O to reduce the number of free parameters. The best simulation result for total magnetization of TiO_{2-x} film at 298 K is shown in Fig. 2. In this fitting we obtain $M_{FM} = 7.0$ emu/cm^3 and small values for anisotropy constants of $K_1 = -1.1 \times 10^3$ erg/cm^3 and $K_2 = 2.0 \times 10^2$ erg/cm^3. The EA was found making an angle of 20° with

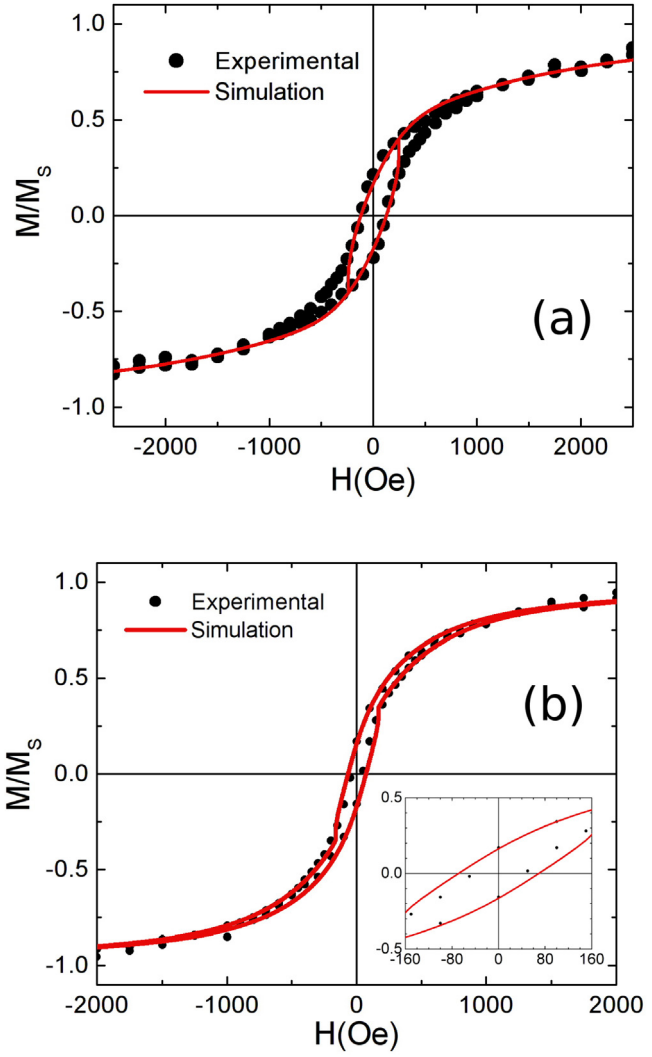

Fig. 2. Experimental (black spheres) and simulation (red lines) results for magnetic hysteresis loop of the TiO_{2-x} film at temperatures (a) 10 K and (b) 300 K. The inner part of the hysteresis loops is shown as inset in the bottom panel.

the normal direction of the film plane, indicating that exists an out-of-plane component of the total magnetization, M_{FM}. Notably, both anisotropy constants are too small and particularly K_2 does not improves significantly the adjustment of the magnetization in the magnetic field intervals between coercive and saturation fields. The M_{FM} value resulting from the fitting is close to the value of 7.0 emu/cm^3 in agreement with values reported in the literature [2].

From the simulated magnetization curve with value of $M_O = 7.0$ emu/cm^3 shown in Fig. 2 results $N_O = 1.6\times10^{21}$/cm^3 for $TiO_{1.95}$. The adjustment of experimental data performed with these parameters leads to that M_{FM} and M_0 contribute on the equal footing for the total saturation magnetization. Therefore, we can conclude that 50% of the V_O sites present in the sample exhibits ferromagnetic behavior and the other 50% contributes to the paramagnetic response, described by the Langevin function. In other words, half of the total moment is due to a magnetically interacting cluster of VO's, whereas the remaining half corresponds to magnetically non-interacting VO's dispersed in the matrix. Surprisingly, the coercive field, H_C, that is often greatly affected by extrinsic factors can be appropriately described in this modeling. The following equation [20,22] describes the coercive field, H_C, obtained from the SW model for small deviations of the hard axis:

$$H_C = \left[\frac{(K_1 + 2K_2)}{M_{FM}}\right]\sin(2\theta_0), \tag{3}$$

where $\theta_0 = \pi/2 - \theta_{EA}$ and $45° \leqslant \theta_0 \leqslant 90°$. By applying the ferromagnetic constants above-defined, one finds $H_C \approx 70$ Oe, which is in good agreement with experimental data at 300 K.

We have also simulated the hysteresis loops measured at 10 K. The same parameters used to simulate the hysteresis loops of the TiO_{2-x} film at 298 K were used to obtain simulation loops at 10 K. In this case, simulated and experimental loops exhibit slightly larger deviations. However, the qualitative adjustment is still reasonably well, as shown in Fig. 2(a). As expected in the present approach, only magnetization PM component described by the Langevin function is the one that contributes most to the magnetization changes with temperature. In spite of our computational efforts, neither changes in the values of magnetizations nor changes in the anisotropy constants K_1 and K_2 promote significant improvements in the simulations at low temperature. We believe that thermal stability of eletronic structure is behind of the robustness of the non-conventional ferromagnetism at low temperatures.

3.2. DFT calculations

To better understand and validate the simulation results, DFT calculations were performed using the all-electron full-potential linearized augmented-plane-wave (FP-LAPW) method, as implemented in the ELK code [23]. In this study, GGA + U exchange-correlation functional within the PBEsol approximation [24] for the non-collinear spin-polarized calculations was used. As pointed out by Shibuya et al. [25], GGA + U calculations can satisfactory describe the DOS of this system. For these calculations we have used U = 5 eV. Such U value is a conciliatory for general features observed in the calculated electronic structure when correlation effects are considered [26]. A grid of 4 k × 4 k × 6 k points in the Brillouin zone was used for the integration in reciprocal space. The total energy and the Kohn-Sham potential convergences were better than 10^{-5} Ha and 10^{-7} Ha, respectively. Fig. 3 shown below was made using the VESTA software [27].

Rutile TiO_2 crystalline structure containing one VO per tetragonal unit cell with the experimental values for lattice parameters $a = 0.45937$ nm and $c = 0.29587$ nm were used in the calculations. A ferromagnetic ground state is found with most of magnetic moment centered at Ti atomic sites with predominance on the first VO neighbors, denoted as T1 with $0.02\mu_B$, and next-nearest VO neighbors, denoted as T2 with $0.01\mu_B$. The interstitial magnetic moment is 0.03 μ_B and remaining magnetic moment per cell is divided among the oxygen sites (-0.01 μ_B) and is oriented in the opposite direction. Hereafter, superscripts 1 and 2 indicate the first and second VO neighbors, respectively. Another important result is that an anisotropic magnetic moment distribution (MMD) contour can be visualized on both Ti atomic sites. Such an anisotropic contour for MMD corroborates with the presence of two different axes of preferential magnetization, one that stays along the crystalline direction [1 1 0] and other that is found about 20°-off the normal of this plane. Therefore, DFT calculations for TiO_2 with high density of VO corroborate with the small magnetic anisotropy observed in our simulations of the magnetic hysteresis loops using free magnetic energy minimization procedure.

Finally, DFT calculations also reveal a significant value of interstitial magnetic moments. This result support the robust ferromagnetism experimentally observed. According to DFT calculations, the magnetic moment per unit cell is approximately 0.05 μ_B, which is in good agreement with value obtained from the simulated of the M versus H curves. Therefore, our simple phenomenological model not only reproduce reasonably well the experimental data but also contains physically consistent elements supported by results of DFT calculations.

The calculated partial DOS for TiO_2 are shown in Fig. 4a–c. Partial spin-resolved DOS of Ti and O sites first (T1 and O1) and next-nearest

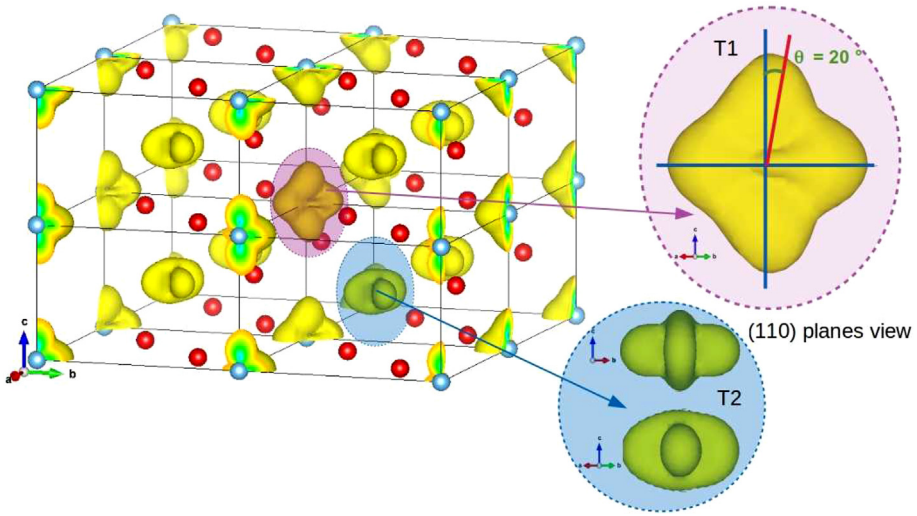

Fig. 3. Representative contour of the magnetic moment distribution (MMD) around atomic sites in the $2\times2\times2$ supercell of rutile TiO_{2-x} with one V_O per unit cell. Blue and red spheres are Ti and O atoms, respectively. The 0.0008 e/Bohr^3 isosurfaces on yellow are shown. The details show the (1 1 0) plane view of the MMD contribution exhibiting an anisotropy contour for the so-called T1 and T2 sites for Ti atoms.

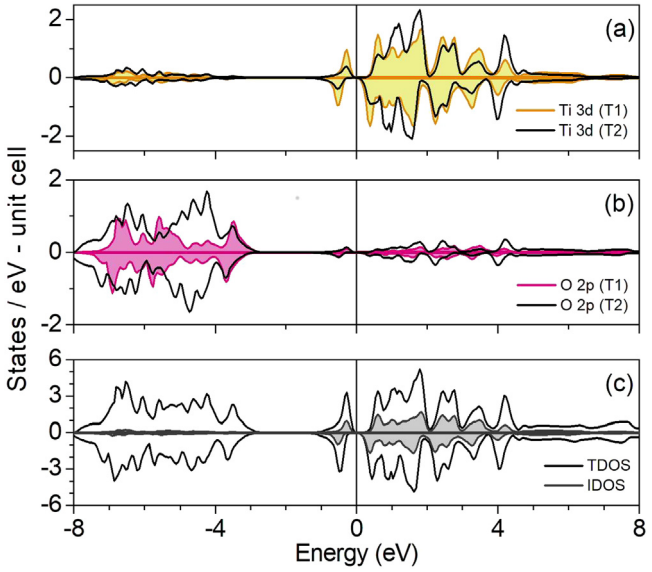

Fig. 4. Calculated DOS for TiO_{2-x} with one VO per unit cell: (a) partial DOS of Ti 3d corresponding to T1 (heavy curves) and T2 (shadowed curves) sites, (b) partial DOS O 2p corresponding to O1 (heavy curves) and O2 (shadowed curves) sites, and (c) interstitial and total DOS.

(T2 and O2) VO neighbors are shown in Fig. 4(a) and (b). Besides, interstitial (IDOS) and total (TDOS) density of states are shown in Fig. 4(c).

In TiO_2, the electrons left behind from released oxygen are distributed in the neighboring titanium sites (from Ti^{4+} to Ti^{3+}) leading to a ground state with Ti3d - O2p hybridization due to this redistribution of charges. As a result, the nearly residual charge distribution generates an interstitial moment around vacancies. In this way, the place occupied by the O^{-2} anion in the regular lattice is taken by one or two "free" electrons in the defective matrix, which minimize the energetic cost of the VO formation. These electrons located on the VO states have a direct effect on the electronic structure of TiO_2 by forming a donor level below the Fermi level. Clearly, the energy level of localized donor states originating from VO is located at 0.1–0.8 eV below the Fermi level ($E_F = 0$). Moreover, the removal of neutral oxygen atoms to form VO's cause the redistribution of the excess electrons among the nearest neighboring Ti atoms around the VO site, and form shallow donor states below the conduction band originating from Ti 3d. These donor states increase with increasing VO, and can even overlap the conduction band in the case of highly defficient matrix [28].

Notably, the more energetic electrons in the defect states have spin polarization inverted in relation to the more accessible states of the bottom of conduction band. This implies that a negative magnetoresistance, as will be seen in the next subsection, in hopping regime can be expected for TiO_{2-x} films at low temperatures, which is indeed experimentally observed.

3.3. Magnetoresistance

To a further exploration of our theoretical approach the electronic transport measurements in TiO_{2-x} films performed with and without the application of an external magnetic field is considered. Basically, the VO magnetic centers embedded in an insulating matrix can be treated as an analogue of a granular system; i.e., a granular magnetic system which often exhibits tunneling magnetoresistance described in terms of the resistance changes when the relative orientation of the magnetization between grains changes by increasing external magnetic field. At low temperature, the conductance of TiO_2 films is described in terms of the variable-range hopping (VRH) conduction theory instead of a simple thermally activated hopping [14]. The VRH conduction process occurs between localized states within "grains" that can be described as VO centers, including the surrounding Ti^{3+} ionic sites, which locally form a polaronic structure.

The four-point technique is the correct procedure to eliminate the contact resistance present in the two-point technique for measuring resistance of a thin film [29]. However, it is often not possible to make a four-point measurement in highly resistive materials, such as TiO_2 at low temperatures, when high voltages are needed to get any measurable current flowing through these materials.

In particular, we reinforce that our measurements were performed at low temperatures (from 5 K to 30 K), when the behavior of conductance follows a VRH regime. In this case, another important point is the number of degree of freedoms which must be controlled during measurements. Four-point measurement of resistance between voltage sense probes is obtained when a current is supplied via two independent probes. The voltage necessary to obtain a measurable current is high and, its value is left free to be whatever is need. Therefore, both temperature and voltage can change during resistance

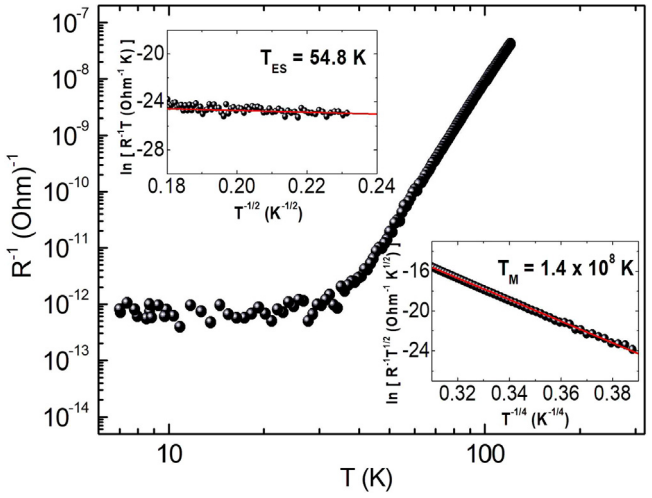

Fig. 5. Logarithm of conductance R^{-1} (black spheres) versus logarithm of temperature T obtained by applying a bias voltage of U = 200 V in the film. The upper (lower) inset shows the characteristic half- (quarter-) power allometric scaling of R^{-1} T (R^{-1} $T^{-1/2}$) in a considerable temperature range below 30 K (above 50 K). Experimental data (black circles) and adjustments (red line) are shown.

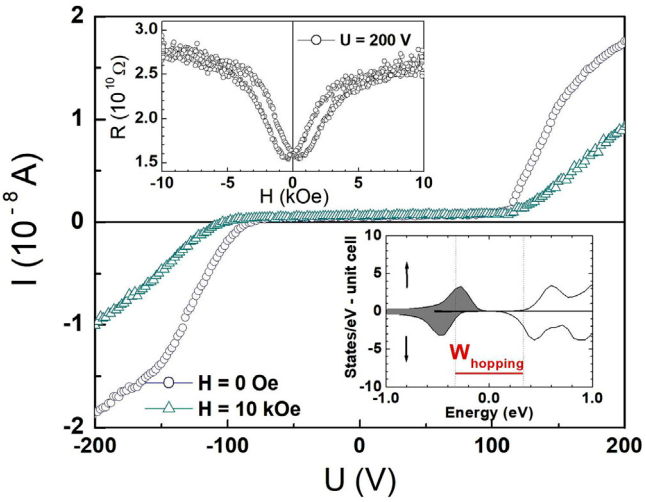

Fig. 6. Characteristic I versus U curve measured at 5 K by scanning voltage U with and without applying a magnetic field along the current flow. Upper inset shows a resistance R versus magnetic field H curve measured maintaining a fixed bias voltage of 200 V. Lower inset shows detail of the total DOS shown in Fig. 4(c) around Fermi level E_F = 0 eV. Occupied defect-states below E_F are represented by filled area of the curves, whereas empty conduction states are given as unfilled area of the curves above E_F. The averaged hopping energy, $W_{hopping}$, is also shown around E_F.

measurements. Otherwise, two-point technique keeps voltage fixed, enabling make an spectroscopic scanning of the electronic states around the Fermi level (rigorously, electrochemical potential). This is quite important for determining the typical distance an electron hops.

According to Fig. 5, temperature dependence of the conductance R^{-1} plotted as $ln\ R^{-1}$ against lnT exhibits a crossover from Mott (M) to Efros-Shklovskii (ES) VRH regime in temperature range between 30 and 50 K; i.e., conductance scales with $T^{-1/2}\exp(-T_M/T)^{-1/4}$ for T < 30 K and $T^{-1}\exp(-T_{ES}/T)^{-1/2}$ for T > 50 K. In both VRH regimes, the characteristic temperatures (T_M and T_{ES}) depend on the electronic density of states (DOS) at Fermi level and the localization length, ξ, of the relevant electronic wavefunction of the donors. Our values of $T_M = 1.4 \times 10^8$ K and T_{ES} = 54.8 K differ only by a factor two from the values found for those samples.

It is worth of note that, the contact resistance in series with sample resistance is certainly small. Notably, the voltage/current slope is almost linear (ohmic) even at 5 K. In addition, our resistance value at room temperature (8 Ohm-cm) is comparable to values reported by other groups for TiO_2 samples with similar stoichiometry (1–20 Ohm-cm) [14,30]. For these reasons, we can presume that measured resistance is mostly due to the electric current lines in the sample slab, which does not significantly disturb estimate values neither for hopping distance nor for magnetoresistance ratio.

The most probable hopping distance, $R_{hopping}$, and hopping energy, $W_{hopping}$, can be estimated as $R_{hopping} \approx \frac{1}{4}\,\xi\,(T_{ES}/T)^{1/2}$ and $W_{hopping} \approx \frac{1}{2}\,k_B\,T\,(T_{ES}/T)^{1/2}$, where the electronic localization length, ξ, refers to the relevant donors and k_B is the Boltzmann constant. Since the carrier density in TiO_2 films mostly corresponding to oxygen vacancies, it is quite reasonable to assume ξ between 2.4 nm and 3.1 nm [14]. Therefore, one finds $R_{hopping} \approx$ 1.7–2.1 nm and $W_{hopping} \approx$ 718.6 meV.

The characteristic current versus voltage (I versus U) curve is shown in Fig. 6. The threshold for increasing current is around 90–100 V for H = 0. When H = 10 kOe is applied the increase of current starts at higher voltage values and their magnitude is significantly lower. This behavior is consistent with ES VRH regime, as expected from the behavior of the resistance as a function of temperature. DC hopping conductance in insulating samples at moderately large magnetic fields commonly shows a field-dependence in both T_{ES} and localization length. Essentially, the typical distance an electron hops, with average hopping energy $W_{hopping}$, is much larger than the average distance between localized states. Thus, in the course of tunneling between the localized states, an electron undergoes multiple elastic scatterings and magnetic-field correction to the localization length could becomes quite appreciable [31].

The measurements of the resistance R vs H in a fixed bias voltage U is shown in the upper inset of Fig. 6. A large increase of the resistance with increasing magnetic field is observed. This negative magnetoresistance can be understood by DFT calculations recalling the spin-resolved total DOS around Fermi shown in the lower inset of Fig. 6. In fact, a negative magnetoresistance is quite plausible under a suitable bias voltage at low temperature to promote electrons hops from spin-up defect states to spin-down conduction states.

Magnetoresistance ratio, defined as $\frac{\Delta R}{R} = 1 - \frac{R(H)}{R(0)} = 1 - \frac{I(0)}{I(H)}$ under a bias voltage U_{bias} = 200 V maintained fixed in the temperature of 5 K, is shown in Fig. 7 after stripping of a small Hall effect signal of raw data. Clearly, a negative magnetoresistance ratio of about 80% is observed.

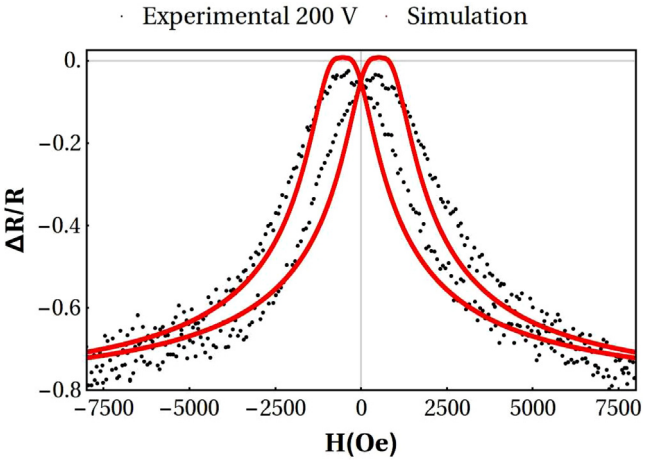

Fig. 7. Longitudinal magnetoresistance curve measured at bias voltage U = 200 V at 5 K for TiO_{2-x} film. Experimental data (solid spheres) and best adjustment (Red solid line) obtained with Helmen-Abeles model are shown.

A direct interplay with our simple approach is possible remembering that mechanism is similarly to the tunneling magnetoresistance observed in granular metal systems with electron hopping through the insulating barrier between localized states associated with VO centers. According to Inoe-Maekawa model [32] a magnetoreisistance ratio given by $P^2\ m^2/\ (1 + P^2\ m^2)$, where P is the spin polarization and m is the relative magnetization of the system, is expected. However, these model explain well the positive magnetoresistance observed on several magnetic granular films. To describe the negative magnetoresistance we recall the earlier work of Helman-Abeles [33]. This work incorporates in the same formalism an extra magnetic energy, E_m, defined as the difference between the magnetic energies of an electron as it tunnels from one grain to another, since when an electron is added to a magnetic grain, the Coulomb interaction between electrons increases both charging and magnetic energies. In this case, there is a magnetoresistance term which is a linear function of the polarization P of the tunneling electrons and from which a negative magnetoresistance can occur. Thus, we consider that magnetoresistance ratio can be expressed as [33]:

$$\frac{\Delta R}{R} = -A(m^2 - m_o^2) \tag{4}$$

where $A = P\ (J/4k_BT)$, P is the polarization of the tunneling electrons with J their effective exchange coupling constant within the ferromagnetic grain centers, k_B is the Boltzmann constant, and $m = L(y)$ in which $y = M_O\ H/k_BT + 3\ (T_m/T)\ L(y)$ with $y \sim 3(T_m/T)$ for $H \sim 0$, since FM contribution provides an extra local field that can orientate the dispersed VO's when the partial intergrain magnetic ordering is taking place. In the above expressions $T_m = E_m/k_B$ corresponds to a characteristic temperature of the intergrain magnetic ordering.

According to Fig. 7, we note that our approach reasonable well reproduces, with two adjustable parameters (PJ and T_m), the main features and the magnitude of the magnetoresistance over a wide magnetic field range. The peak of magnetoresistance at $H_p = 240$ Oe enable us to make an estimate of using the relation $T_m \approx M_O\ \Omega_O\ H_p/3k_B$, where M_O is the total magnetization of the paramagnetic centers and Ω_0 is the average volume of an isolated VO. Using $M_O = 7.0$ emu/cm^3 and $\Omega_0 \approx 62$ Å^3, one finds $T_m \approx 2.5$ K, which explain why the magnetoresistance is observed only at low temperatures. If we consider spin-polarization of the magnetic centers having $P = -1$, the effective exchange energy J becomes about three times the thermal energy at 5 K. Therefore, the large negative magnetoresistance observed at low temperatures and high bias voltage can be reasonably explained within our simple approach and our parametrization can be supported by calculated DOS.

4. Conclusions

In summary, we demonstrated that quite reasonable and simple phenomenological approach can be used to understand non-conventional ferromagnetism and magnetoresistance in TiO_{2-x} films.

The standard minimization method of the free magnetic energy leads to magnetization curves and simple linear approximation of magnetoresistance in VRH regime uses a minimal number of free paramaters which are consistently supported by calculations performed within density functional density theoretical framework.

Our present results encourage the application of simple and standard procedures to describe non-conventional ferromagnetism in others oxygen-defective metal oxide systems, whose multifunctional properties are promising for several technological applications.

Declaration of Competing Interest

The authors declare that they have no known competing financial interests or personal relationships that could have appeared to influence the work reported in this paper.

Acknowledgements

The authors thank the Brazilian funding agency CNPq and FAPESP (2017/24995-2 and 2013/07296-2) for partial financial support, and our special thanks to Dr. Y. Zheng who produced the samples.

Appendix A. Supplementary data

Supplementary data associated with this article can be found, in the online version, athttps://doi.org/10.1016/j.jmmm.2019.166068.

References

[1] N.H. Hong, J. Sakai, N. Poirot, V. Briz, Phys. Rev. B 73 (2006) 132404 .
[2] S.D. Yoon, Y. Chen, A. Yang, T.L. Goodrich, X. Zuo, D.A. Arena, K. Ziemer, C. Vittoria, V.G. Harris, J. Phys.: Condens. Matter 18 (2006) L355–L361.
[3] C. Sudakar, P. Kharel, R. Suryanarayanan, J.S. Thakur, V.M. Naik, R. Naik, G. Lawes, J. Magn. Magn. Mater. 320 (2008) L31–L36.
[4] H. Peng, J. Li, S.-S. Li, J.-B. Xia, Phys. Rev. B 79 (2009) 092411 .
[5] Y.R.P.D. Kim, J. Hong, K.J. Kim, J. Phys.: Condens. Matter 21 (2009) 195405 .
[6] K.S. Yang, Y. Dai, B.B. Huang, Y.P. Feng, Phys. Rev. B 81 (2010) 033202 .
[7] Y.Y.H.X. Wang, Z.C. Zong, J. Appl. Phys. 115 (2014) 233909 .
[8] S.-J. Hu, S.-S. Yan, L.-M. Mei, Phys. Status Solidi RRL 3 (5) (2009) 148–150.
[9] A.K. Rumaiza, B. Ali, A. Ceylan, M. Boggs, T. Beebe, S.I. Shah, Solid State Commun. 144 (2007) 334–338.
[10] K.I.B. Santara, P.K. Giri, M. Fujii, Nanoscale 5 (2013) 5476.
[11] X.-H. Wei, R. Skomski, D.J. Sellmyer, IEEE Trans. Magn. 45 (10) (2009) 4089–4091.
[12] S. Zhou, E. Cizmar, K. Potzger, M. Krause, G. Talut, M. Helm, J. Fassbender, S.A. Zvyagin, J. Wosnitza, H. Schmidt, Phys. Rev. B 79 (2009) 113201 .
[13] C.D. Valentin, G. Pacchioni, A. Selloni, J. Phys. Chem. C 113 (2009) 20543–20552.
[14] A. Yildiz, S.B. Lesesivdin, M. Kasap, D. Mardare, J. Non-crystal. Solids 354 (2008) 4944–4947.
[15] J. Varalda, C. Dartora, A. de Oliveira, B. Ortiz, W.A. Vodungbo, F. Marangolo, M. Vidal, Y. Zheng, G. Cabrera, D. Mosca, Phys. Rev. B 83 (2011) 045205 .
[16] J. Varalda, W.A. Ortiz, A.J.A. de Oliveira, B. Vodungbo, Y.-L. Zheng, D. Demaille, M. Marangolo, D.H. Mosca, J. Appl. Phys. 101 (2007) 014318 .
[17] B. Vodungbo, Y. Zheng, M. Marangolo, D. Demaille, J. Varalda, J. Phys.: Condens. Matter 19 (2007) 116205 .
[18] S. Chikazumi, Physics of Ferromagnetism, Clarendon Press, Oxford, 1997.
[19] V. Paes, I. Graff, J. Varalda, V. Etgens, D. Mosca, J. Phys.: Condens. Matter 25 (2013) 046003 .
[20] E. Stoner, E.P. Wohlfarth, Philos. Trans. R. Soc. A 240 (826) (1948) 599–642.
[21] V.Z.C. Paes, J. Varalda, P. Schio, J.T. Matsushima, E.C. Pereira, A.J.A. de Oliveira, D.H. Mosca, J. Mater. Res. 31 (14) (2016) 2058–2064.
[22] J. Wang, S. Yang, J. Gong, M. Xu, M. Adil, Y. Wang, Y. Zhang, X. Song, H. Zeng, Phys. Chem. Chem. Phys. 17 (15) (2015) 10250–10256.
[23] K. Dewhurst, The elk code,http://elk.sourceforge.net/.
[24] J.P. Perdew, A. Ruzsinszky, G.I. Csonka, O.A. Vydrov, G.E. Scuseria, L.A. Constantin, X. Zhou, K. Burke, Phys. Rev. Lett. 100 (2008) 136406 .
[25] Shibuya, J. Phys.: Condens. Matter 24 (2012) 435504 .
[26] A.M.-G.M.E. Arroyo-de Dompablo, M. Taravillo, J. Chem. Phys. 135 (2011) 054503 .
[27] K. Momma, F. Izumi, J. Appl. Cryst. 44 (2011) 1272–1276.
[28] X. Pan, M.-Q. Yang, X. Fu, N. Zhang, Y.-J. Xu, Nanoscale 5 (2013) 3601.
[29] M.B. Heaney, Electrical conductivity and resistivity, in: John G. Webster (Ed.), Electrical Measurement, Signal Processing, and Displays, 2003.
[30] Y.L.Z. et al., AIP Adv. 2 (2012) 012129.
[31] H.L. Zhao, B.Z. Spivak, M.P. Gelfand, S. Feng, Phys. Rev. B 44 (1991) 10760–10767.
[32] J. Inoue, S. Maekawa, Phys. Rev. 53 (R11) (1996) 927.
[33] J.S. Helman, B. Abeles, Phys. Rev. Lett. 37 (1976) 1429.